

# High-Precision Dual-Loop Position Control of an Asymmetric Bilateral Linear Hybrid Switched Reluctance Motor

J. F. Pan<sup>1</sup>, Yu Zou<sup>1,2</sup>, Guangzhong Cao<sup>1</sup>, Norbert C. Cheung<sup>2</sup>, and Bo Zhang<sup>1</sup>

<sup>1</sup>Shenzhen Key Laboratory of Electromagnetic Control, Shenzhen University, Shenzhen 518060, China

<sup>2</sup>Department of Electrical Engineering, The Hong Kong Polytechnic University, Hong Kong

In this paper, to enhance the machine performance and realize a high-precision position control performance, a dual-loop position controller is employed for the asymmetric bilateral linear hybrid switched reluctance motor (ABLHSRM). Machine characteristics are investigated by finite-element method. The dual-loop controller is constructed by employing a tradition proportional–integral differential velocity controller as the inner loop and a fuzzy proportional differential (PD) controller for the outer loop. Experimental results demonstrate that both the position control performance and the velocity control performance under the dual-loop control algorithm are superior to the single-loop PD position control strategy. An absolute steady-state error of 4  $\mu\text{m}$  can be achieved under the dual-loop control strategy. Performance comparison from the ABLHSRM and its asymmetric bilateral linear switched reluctance counterpart with the same dimensions are carried out. Position tracking results show that the rise time is improved for the proposed ABLHSRM under the proposed control scheme.

**Index Terms**—Dual-loop control, finite-element method (FEM), fuzzy, position control.

## I. INTRODUCTION

LINEAR motors, as direct-drive actuators, have been quickly developed within recent years, and now, they are widely applied in the industrial drives for position control applications, such as automatic soldering, carving, embroidery machines, and so on [1]. Linear permanent magnetic motors (LPMs) are the mainstream of the contemporary market due to their considerable force output with high power density and efficiency [2]. However, the high cost of permanent magnets (PMs) restricts the wide use of LPMs, since they employ a considerable amount of PMs or complicated winding schemes for the magnetic circuit construction. On the other hand, the cogging force ripples are another unwanted feature of the LPMs, because the ripples often deteriorate the accuracy of position control [3].

The linear switched reluctance motor (LSRM), owing to its simple and low-cost machine topology, is one of the potential candidates for high-precision position control applications as well. However, the magnetic circuits of pure LSRMs are only composed of silicon-steel plates, and pure LSRMs are limited to some special applications due to their inherent low propulsion force output and efficiency, especially at low speed [4].

In recent years, the idea of flux-switching is proposed by the introduction of appropriate amount of PMs at appropriate places in the machines [5]. Some studies on the linear hybrid switched reluctance machines (LHSRMs) have been carried out. Since an LHSRM inherits the advantages of both an LSRM and an LPM, the efficiency and force output performance can be enhanced and the cost can be reduced in

an LHSRM at the same time [6]–[8]. In [6], a hybrid type of linear motor is designed to reduce the detent force, and a hybrid linear flux switching permanent magnet motor is presented, in order to replace rare-earth magnets by ferrite magnets [7]. Hahn *et al.* [8] investigated the flux densities at the stator and the mover teeth, by selecting the proper PMs with specified magnetization field values. However, these linear hybrid machines discussed above have the unavoidable disadvantages that the main magnetic circuits are separated by the embedded PMs [5]. This method inevitably increases the total air-gap length of the machine, since the permeability of the PMs is comparable with that of the air gap. In addition, this arrangement often increases the reluctance of the motors and decreases the number of flux lines in the main magnetic circuits [9].

Research work on optimized mechanical design and advanced control implementation for LSRMs has also been carried out. An asymmetric LSRM (ALSRM) has been proposed to improve the force output performance, and enhance the response of the machine, by decreasing the weight of the moving part [10]. To realize a smooth control, force distribution functions have been devised to linearize nonlinear inductance profiles for LSRMs [11], [12].

To avoid the above-mentioned influence from separated embedded PMs to the main magnetic circuits, in this paper, an asymmetric, bilateral linear hybrid switched reluctance motor (ABLHSRM) is proposed. The contribution includes the following aspects. First, without the modification of the existing machine structure and for the full utilization of the stator leg slot region, only one PM is inserted into the stator leg slot for any phase, in order to enhance the machine's efficiency and force output performance. Second, to inspect the position control performance of the proposed machine, a dual-loop position control scheme incorporating velocity and position control strategy is developed. The simple yet effective proportional–integral differential (PID) controller is employed for speed regulation in the inner loop.

Manuscript received March 20, 2015; revised June 15, 2015; accepted June 18, 2015. Date of publication June 19, 2015; date of current version October 22, 2015. Corresponding author: B. Zhang (e-mail: zhangbo@szu.edu.cn).

Color versions of one or more of the figures in this paper are available online at <http://ieeexplore.ieee.org>.

Digital Object Identifier 10.1109/TMAG.2015.2447522

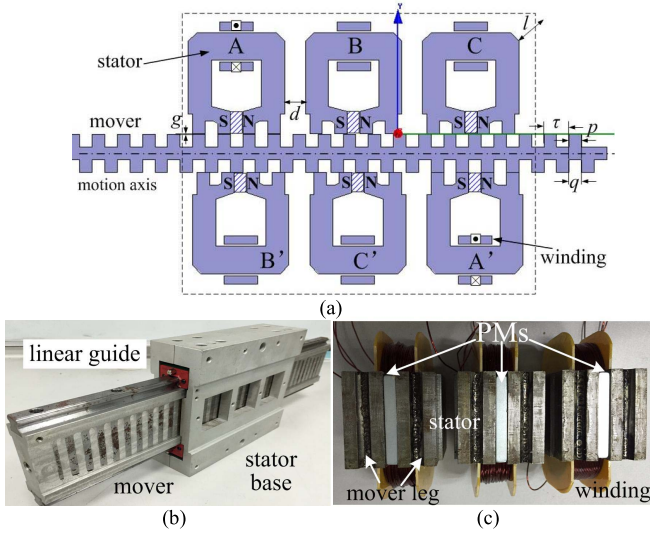


Fig. 1. (a) Machine schematic, (b) stators, and (c) mover and stator base.

TABLE I  
MAJOR SPECIFICATIONS OF THE ABLHSRM

Parameter	Value
Number of phase windings ( $N$ )	200 turns
Phase division ( $d$ )	10 mm
Air gap ( $g$ )	0.3 mm
Stroke length	350 mm
Stack length ( $l$ )	100 mm
Stator/mover pole width ( $p$ )	6 mm
Stator/mover slot width ( $q$ )	20 mm
Pole-pitch ( $\tau$ )	12 mm
Dimensions of PMs	$4.5 \times 5 \times 100$ mm <sup>3</sup>
$B_r$ of PMs	1.2 T
$H_c$ of PMs	652 kA/m
Mover mass	2.5 Kg

Fuzzy proportional differential (PD) position regulator is applied for the outer loop control to realize high-precision position control performance [13].

## II. CHARACTERISTIC ANALYSIS

### A. Mechanical Structure

This motor adopts an asymmetric structure of the mover [10]. As shown in Fig. 1(a), there are three phases named as phase AA', BB', and CC', and each phase has two coils concentrated on two stators. Six stators are fixed on an aluminum base connected by a pair of linear guides, as shown in Fig. 1(b).

As shown in Fig. 1(c), one PM is inserted into the middle of each stator legs, and there are six PMs in the machine altogether. The PMs are arranged in the manner so that the magnetization direction is opposite to that of phase current excitation. Major specifications are listed in Table I.

### B. Characteristic Analysis

Although the PMs are embedded into the stators, flux lines only circulate through the stators and there are no flux lines in the air gap or the mover at zero current excitation, and therefore, the cogging force is zero. For any one stator, as the current is increased, the flux lines from the PM are first

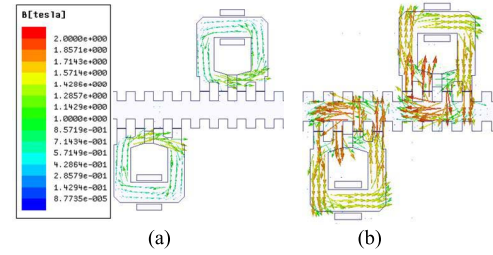


Fig. 2. Flux distribution at (a) zero current and (b) 5 A.

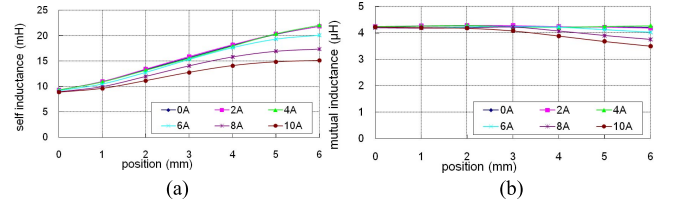


Fig. 3. (a) Self-inductance and (b) mutual inductance profiles.

counteracted by those from the external current. Then, some of the flux lines from the PM are compelled to the mover as current increases. Last, the total flux lines pass through the air gap and arrive at the mover. Flux distribution contours for zero current, and the level of 5 A are plotted, as shown in Fig. 2(a) and (b). It can be seen that the flux density can be strengthened by the introduction of the PM for each phase.

The equation that governs the machine behavior can be expressed as

$$u = R \cdot i + L \cdot \frac{di}{dt} \quad (1)$$

$$F = M \frac{d^2x}{dt^2} + D \frac{dx}{dt} + F_l \quad (2)$$

where  $u$  and  $i$  are the terminal voltage and phase current.  $R$  and  $L$  are the phase resistance and inductance, respectively.  $F$  and  $F_l$  are the propulsion and load force.  $M$  and  $D$  are the mass of the mover and damping coefficient, respectively.  $x$  is the displacement.

Since the internal reluctance is approximately equal to that of air, the ABLHSRM virtually has identical self-inductance and mutual inductance values versus current and position in spite of embedded PMs. According to the finite-element method (FEM), the self-inductance and mutual inductance profiles are calculated with the results shown in Fig. 3. It can be seen that the self-inductance is increased with respect to the displacement from the unaligned position (0 mm) to the aligned position (6 mm). Meanwhile, the relative ratio values from the mutual inductance to the self-inductance fall into the range of 5%. Thereby, the coupling effect between adjacent phases can be considered negligible.

According to the basic magnetic structure, reluctance definitions for any one stator, the air gap, and the mover can be found in Fig. 4(a).  $R_s$  represents the total reluctance of the stator yoke, leg, and teeth and  $R_m$  is the total reluctance for the mover teeth and yoke.  $R_p$  and  $R_g$  are the values of internal reluctance of the PM and the air gap, respectively. The equivalent magnetic circuit can thus be represented, as shown in Fig. 4(b).

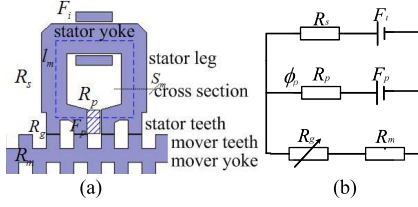


Fig. 4. (a) Equivalent magnetic circuit and (b) its representation.

$F_i$  and  $F_p$  are the magnetic potential of the external current excitation and the PM, respectively. If the external excitation is zero, the flux lines are generated from the PM by  $F_p$ , passing through the reluctance  $R_s$  in the stator only. There is no interactive force from the mover to the stator from the machine. It enjoys a free cogging force at zero current excitation.  $F_p$  can be expressed as

$$F_p = \phi_p \cdot (R_p + R_s) \quad (3)$$

where  $\phi_p$  is the magnetic flux generated by the PM only. If the magnetic field is established by the current excitation and the direction is opposite to that of the PM, it is clear that the flux lines from the current excitation first weaken those generated from the PM, and then the flux lines of the PM are forced to travel along the air gap, stator yoke, and teeth. The magnetic field in the stator is thus enforced, and the resultant flux lines circulate through the stator yoke, leg and teeth, mover teeth and yoke, and the air gap. Therefore, an enhanced magnetic flux with less leakage can be achieved. The magnetic flux in the air gap  $\phi_g$  can be expressed as

$$\phi_g = \phi_i + K\phi_p \quad (4)$$

where  $\phi_i$  is the flux produced by the current and  $K\phi_p$  is generated by the PM. The value of  $K$  depicts the portion of PM flux lines that successfully reach the mover by crossing the air gap. It is clear that  $K$  depends on the total magnetic reluctance, which changes with respect to the displacement  $x$  of the mover platform. The value of  $K$  is

$$K(x) = \frac{R_p}{R_p + R_s / (R_g(x) + R_m)}. \quad (5)$$

Neglecting magnetic saturation, propulsion force output of one phase can be characterized as

$$F = \frac{1}{2} \cdot (i + i_p)^2 \cdot \frac{dL}{dx} \quad (6)$$

where  $i$  is the excitation current,  $L$  is the self-inductance, and  $i_p$  is the current that produces the equivalent force from the PM, and according to (4),  $i_p$  can thus be calculated by

$$i_p = \frac{K\phi_p}{\phi_i} \cdot i. \quad (7)$$

With embedded PMs, it is clear that flux density is increased, so that the propulsion force output is enhanced. Force values versus current and displacement are measured by a commercial load cell with profiles for the ABLHSRM and its ALSRM counterpart with the same dimensions containing no PMs, as shown in Fig. 5. It can be concluded that the propulsion force output values of the ABLHSRM are higher than those from the ALSRM counterpart.

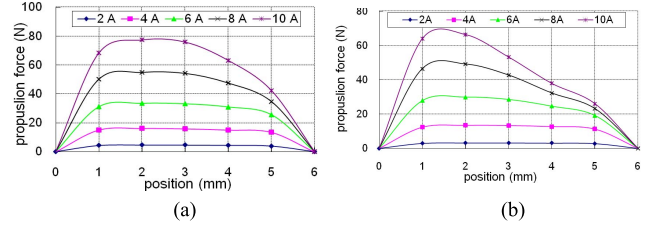


Fig. 5. Measured force outputs of (a) the ABLHSRM and (b) ALSRM.

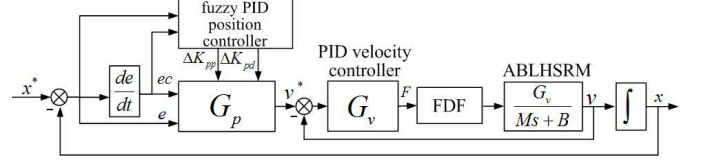


Fig. 6. Dual-loop control block diagram.

### III. DUAL-LOOP CONTROL SCHEME

Considering that the bandwidth of the current control loop is much higher than that of the speed or position, the transfer function of the velocity control and position control loop can be expressed as

$$\frac{v}{v^*} = \frac{G_v}{M \cdot s + B + G_v} \quad (8)$$

$$\frac{x}{x^*} = \frac{G_p \cdot G_v}{(Ms^2 + (B + G_v)s + G_p G_v)} \quad (9)$$

where  $v^*$  and  $x^*$  are the velocity and position references, and  $v$  and  $x$  are the velocity and position feedbacks.  $G_v$  and  $G_p$  represent the gains for the position and velocity loops. These include the  $P$ ,  $I$ , and  $D$  gains for the velocity loop and  $P$  and  $D$  gains for the position loop.

The PID and the fuzzy PD algorithms are employed for the velocity and the position loops with the force distribution function proposed in [12]. The control block diagram is shown in Fig. 6. Updated  $P$  and  $D$  gains  $K_{pp}$  and  $K_{pd}$  of the position controller are calculated recursively based on the fuzzy logic, and they can be represented as

$$\begin{cases} K_{pp} = K_{pp0} + \Delta K_{pp} \\ K_{pd} = K_{pd0} + \Delta K_{pd} \end{cases} \quad (10)$$

where  $\Delta K_{pp}$  and  $\Delta K_{pd}$  are the incremental  $P$  and  $D$  gains with the initial gain values of  $K_{pp0}$  and  $K_{pd0}$ . The fuzzy controller is designed based on the position error  $e$  and its deviation  $ec$ . Both of them are continuously updated and modified in real time, according to the fuzzy control rules on meeting the control requirements. For the ABLHSRM, the domain of the fuzzy set is determined as  $e, ec: \{-6 \ -4 \ -2 \ 0 \ 2 \ 4 \ 6\}$  with the word set  $\{NB \ NM \ NS \ ZO \ PS \ PM \ PB\}$ . The corresponding linguistic variable fuzzy set consists of negative large, negative middle, negative small, zero, positive small, positive middle, and positive big. The parameter setting rules can be summarized as follows [14].

- 1) If  $e$  is big, in order to achieve a fast dynamic response, values of  $K_{pp}$  and  $K_{pd}$  should be set relatively bigger and smaller, respectively.

TABLE II  
FUZZY RULE

$\Delta K_{pp} \backslash \Delta K_{pd}$ $e$	$ec$		NB	NM	NS	ZO	PS	PM	PB
NB	PB\PS $\ominus$	PB\PS $\ominus$	PMPB $\ominus$	PMPB $\ominus$	PS\PM $\ominus$	PS\PS $\ominus$	ZO\PS $\ominus$		
NM	PB\PS $\ominus$	PB\PS $\ominus$	PMPB $\ominus$	PS\PM $\ominus$	PS\PM $\ominus$	ZO\PS $\ominus$	ZO\ZO $\ominus$		
NS	PM\ZO $\ominus$	PM\PS $\ominus$	PMPM $\ominus$	PS\PM $\ominus$	ZO\PS $\ominus$	ZO\PS $\ominus$	ZO\ZO $\ominus$		
ZO	PM\ZO $\ominus$	PM\PS $\ominus$	PS\PS $\ominus$	ZO\PS $\ominus$	PS\PM $\ominus$	PM\PS $\ominus$	PM\ZO $\ominus$		
PS	ZO\ZO $\ominus$	ZO\PS $\ominus$	ZO\PS $\ominus$	PS\PM $\ominus$	PM\PS $\ominus$	PM\PS $\ominus$	PM\ZO $\ominus$		
PM	ZO\ZO $\ominus$	ZO\PS $\ominus$	PS\PM $\ominus$	PS\PM $\ominus$	PMPB $\ominus$	PM\PS $\ominus$	PB\PS $\ominus$		
PB	ZO\PS $\ominus$	PS\PS $\ominus$	PMPM $\ominus$	PMPB $\ominus$	PMPB $\ominus$	PB\PS $\ominus$	PB\PS $\ominus$		

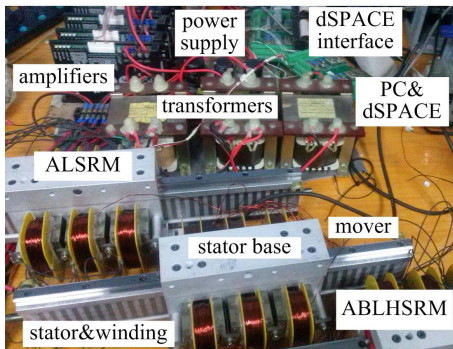


Fig. 7. Experimental setup.

- 2) If  $e$  is medium,  $K_{pp}$  can be set as a small value and  $K_{pd}$  is big to obtain a small overshoot from the position response.
- 3) When the position approaches the reference value,  $e$  becomes small.  $K_{pp}$  is small to avoid system oscillation. Meanwhile, according to the value of  $ec$ , if the value of  $ec$  is small, then the value of  $K_{pd}$  can be bigger; if  $ec$  is big, the value of  $K_{pd}$  can be a small value.

According to the setting principles of  $K_{pp}$  and  $K_{pd}$ , the fuzzy rules table can be obtained, as shown in Table II, and the center average defuzzification method is employed [14].

#### IV. EXPERIMENTAL RESULTS

The whole experiment is conducted in real time, and the sampling frequency values for velocity and position control loop are set as 2 and 1 KHz, respectively. The experimental setup is shown in Fig. 7, which is mainly composed of the ABLHSRM and the ALSRM with the same dimensions without PMs, drives, power supply with transformers, and a dSPACE control card. The current drives are three commercial amplifiers capable of inner current regulation at a sampling rate of 10 KHz. Position feedback is accomplished by a linear magnetic encoder with the resolution of  $1 \mu\text{m}$ .

The frequency and amplitude of the position command for the ALSRM are first set as 1 Hz and 20 mm to observe steady-state behaviors under the single-loop PD position control and the dual-loop regulator, respectively. Control parameters are

TABLE III  
PARAMETERS OF PID CONTROLLERS

parameter	$G_p$	$G_v$
P	0.390	0.759
I	-	0.317
D	0.071	0.002

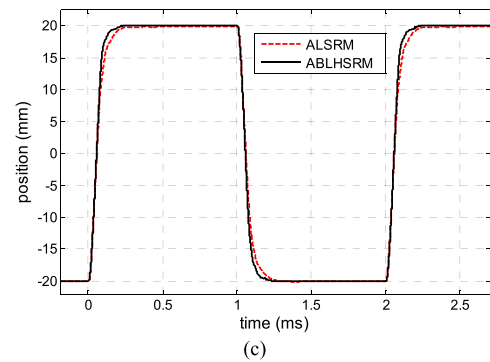
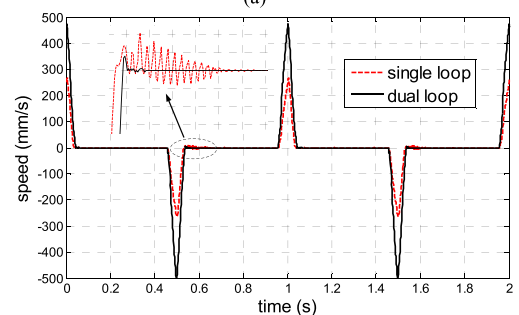
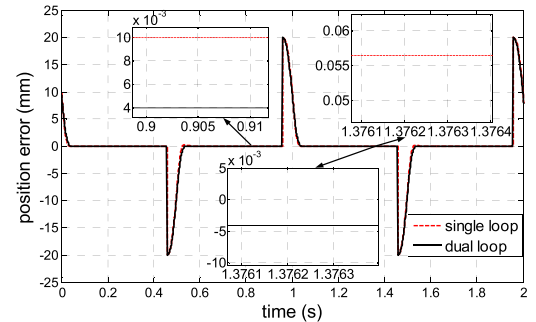


Fig. 8. (a) Position error response. (b) Velocity tracking response. (c) Position response comparison from ABLHSRM and ALSRM.

regulated according to the same rise time of position response, and the values are tabulated in Table III.

The position error response and speed response profiles can be found in Fig. 8(a) and (b), respectively. It is clear that the dynamic behaviors from the two controllers are close to each other. However, it can be observed from the steady response that the behaviors are not identical. For the single-loop position algorithm under PID, the steady-state error values are quite different with 0.01 and 0.057 mm. For the dual-loop controller, the steady-state error values are identical with an absolute value of  $4 \mu\text{m}$ . This is because the fuzzy PID regulator takes the initial parameter values from Table III and modifies the incremental  $P$  and  $D$  gains in real time, according to current position error information. The dynamic velocity response

waveforms demonstrate that a faster response can be achieved if the inner velocity control loop is employed. The response under the single-loop control alone also proves that significant jittering occurs during sharp velocity transitions.

To demonstrate that the ABLHSRM is superior to the ALSRM with the same dimensions, performance comparison of position control under the proposed dual-loop controller is carried out. As shown in Fig. 8(c), the dynamic tracking response under square waveform command with the amplitude of 20 mm and the frequency of 2 Hz, and the rise time for the ABLHSRM can be calculated as 0.04 ms, faster than the ALSRM with the same dimensions containing no PMs.

## V. CONCLUSION

This paper first inspects a novel hybrid ALSRM by the simple utilization of PMs embedded into the stator leg slots. This arrangement does not affect the air-gap length or increase the reluctance of the main magnetic circuits from the existing pure ALSRM without PMs. Machine properties, including inductance and force output, are analyzed by the FEM, and the results demonstrate that the machine has a negligible mutual inductance effect between adjacent phases and a better force output performance, when compared with the ALSRM counterpart with the same dimensions without PMs. Last, this paper presents a dual-loop control system for the hybrid machine. Experimental results indicate that the steady-state error of  $\pm 4 \mu\text{m}$  can be achieved under the dual-loop control strategy. Meanwhile, a faster rise time of 0.04 ms can be enjoyed for the ABLHSRM under the dual-loop controller when compared with its ALSRM counterpart.

## ACKNOWLEDGMENT

This work was supported in part by National Natural Science Foundation of China under Project 51477103, in part by Guangdong Natural Science Foundation under Project S2014A030313564, in part by Shenzhen Government under Grant JCYJ20130329144017199, and in part by PolyU Research Fund under Grant G-YK63.

## REFERENCES

- [1] R. Cao, M. Cheng, C. Mi, W. Hua, and W. Zhao, "Comparison of complementary and modular linear flux-switching motors with different mover and stator pole pitch," *IEEE Trans. Magn.*, vol. 49, no. 4, pp. 1493–1504, Apr. 2013.
- [2] J. X. Jin, L. H. Zheng, Y. G. Guo, and J. G. Zhu, "Performance characteristics of an HTS linear synchronous motor with HTS bulk magnet secondary," *IEEE Trans. Ind. Appl.*, vol. 47, no. 6, pp. 2469–2477, Nov./Dec. 2011.
- [3] C.-C. Hwang, P.-L. Li, and C.-T. Liu, "Optimal design of a permanent magnet linear synchronous motor with low cogging force," *IEEE Trans. Magn.*, vol. 48, no. 2, pp. 1039–1042, Feb. 2012.
- [4] J.-H. Park, S.-M. Jang, J.-Y. Choi, S.-Y. Sung, and I.-J. Kim, "Dynamic and experimental performance of linear-switched reluctance machine with inductance variation according to airgap length," *IEEE Trans. Magn.*, vol. 46, no. 6, pp. 2334–2337, Jun. 2010.
- [5] G.-A. Capolino and A. Cavagnino, "New trends in electrical machines technology—Part I," *IEEE Trans. Ind. Electron.*, vol. 61, no. 8, pp. 4281–4285, Aug. 2014.
- [6] C.-F. Wang, J.-X. Shen, Y. Wang, L.-L. Wang, and M.-J. Jin, "A new method for reduction of detent force in permanent magnet flux-switching linear motors," *IEEE Trans. Magn.*, vol. 45, no. 6, pp. 2843–2846, Jun. 2009.
- [7] C.-C. Hwang, P.-L. Li, and C.-T. Liu, "Design and analysis of a novel hybrid excited linear flux switching permanent magnet motor," *IEEE Trans. Magn.*, vol. 48, no. 11, pp. 2969–2972, Nov. 2012.
- [8] M. Hahn, M. Bedenbecker, and H. H. Gatzert, "Evaluation of a linear hybrid microstep motor by means of magnetic flux measurements," *IEEE Trans. Magn.*, vol. 43, no. 6, pp. 2588–2590, Jun. 2007.
- [9] R. Cao, M. Cheng, C. Mi, W. Hua, and W. Zhao, "A linear doubly salient permanent-magnet motor with modular and complementary structure," *IEEE Trans. Magn.*, vol. 47, no. 12, pp. 4809–4821, Dec. 2011.
- [10] J. F. Pan, Y. Zou, and G. Cao, "An asymmetric linear switched reluctance motor," *IEEE Trans. Energy Convers.*, vol. 28, no. 2, pp. 444–451, Jun. 2013.
- [11] X. Xue, K. E. Cheng, Z. Zhang, J. Lin, and N. Cheung, "A novel method to minimize force ripple of multimodular linear switched reluctance actuators/motors," *IEEE Trans. Magn.*, vol. 48, no. 11, pp. 3859–3862, Nov. 2012.
- [12] J. F. Pan, N. C. Cheung, and Y. Zou, "An improved force distribution function for linear switched reluctance motor on force ripple minimization with nonlinear inductance modeling," *IEEE Trans. Magn.*, vol. 48, no. 11, pp. 3064–3067, Nov. 2012.
- [13] Y. Wang, "A novel fuzzy controller for switched reluctance motor drive," in *Proc. IEEE 2nd Int. Conf. Inf. Comput. Sci. (ICIC)*, May 2009, pp. 55–58.
- [14] H.-C. Yu, T.-C. Chen, and C.-S. Liu, "Adaptive fuzzy logic proportional-integral-derivative control for a miniature autofocus voice coil motor actuator with retaining force," *IEEE Trans. Magn.*, vol. 50, no. 11, Nov. 2014, Art. ID 8203204.